Earth and Planetary Science Letters 333–334 (2012) 91–100

Contents lists available at SciVerse ScienceDirect

Earth and Planetary Science Letters

journal homepage: www.elsevier.com/locate/epsl

Sources of shaking and flooding during the Tohoku-Oki earthquake: A mixture of rupture styles

Shengji Wei [a,*], Robert Graves [b], Don Helmberger [a], Jean-Philippe Avouac [a], Junle Jiang [a]

[a] Seismological Laboratory, Division of Geological and Planetary Sciences, California Institute of Technology, Pasadena, CA 91125, USA
[b] U.S. Geological Survey, 525 S. Wilson Avenue, Pasadena, CA 91106, USA

ARTICLE INFO

Article history:
Accepted 6 April 2012
Editor: P. Shearer

Keywords:
Tohoku-Oki earthquake
finite fault
strong motion
tsunami
high-rate GPS

ABSTRACT

Modeling strong ground motions from great subduction zone earthquakes is one of the great challenges of computational seismology. To separate the rupture characteristics from complexities caused by 3D sub-surface geology requires an extraordinary data set such as provided by the recent Mw9.0 Tohoku-Oki earthquake. Here we combine deterministic inversion and dynamically guided forward simulation methods to model over one thousand high-rate GPS and strong motion observations from 0 to 0.25 Hz across the entire Honshu Island. Our results display distinct styles of rupture with a deeper generic interplate event (~Mw8.5) transitioning to a shallow tsunamigenic earthquake (~Mw9.0) at about 25 km depth in a process driven by a strong dynamic weakening mechanism, possibly thermal pressurization. This source model predicts many important features of the broad set of seismic, geodetic and seafloor observations providing a major advance in our understanding of such great natural hazards.

1. Introduction

Large subduction zone earthquakes pose one of the greatest natural hazards to mankind, either by strong shaking and/or flooding (tsunami). Fortunately, earthquakes with magnitude greater than Mw9 are very rare and the conditions under which such devastating events can happen remain unclear. Although the general concept of interplate thrust faulting breaking locked zones is well established (Fig. 1A), the details of the physical process determining rupture characteristics are less well understood. Most of our understanding of these events comes from long period seismology, primarily by the modeling of global observations where mechanisms and moment estimates have proven to be quite accurate when compared with geodetic data (i.e. Lay and Bilek, 2006). Unfortunately, accurate determination of epicenters and rupture pattern details are less resolved because these events occur primarily beneath the oceans with limited near-source data (Chu et al., 2011). The wealth of data available for the 2011 Mw9.0 Tohoku-Oki earthquake (i.e. Sato et al., 2011) which occurred offshore northern Honshu (Fig. 1) provides a unique opportunity to investigate the details of a large megathrust ruptures and those related to its devastating effects (ground shaking and tsunami).

So far, a number of slip models have been derived for this event by using geodetic data (Ozawa et al., 2011; Yue and Lay, 2011), teleseismic data (Hayes, 2011; Ide et al., 2011; Shao et al., 2011; Yagi and Fukahata, 2011), strong motion data (Kurahashi and Irikura, 2011; Suzuki et al., 2011; Yoshida et al., 2011), tsunami data (Fujii et al., 2011; Hayashi et al., 2011; Lay et al., 2011; Maeda et al., 2011; Saito et al., 2011; Tsushima et al., 2011; Yamazaki et al., 2011), and joint inversion of multiple data sets (Ammon et al., 2011; Koketsu et al., 2011; Lee et al., 2011; Simons et al., 2011; Yokota et al., 2011). In most of these previous studies, the temporal evolution of slip is modeled using multiple time windows in the inversion procedure. The benefit of such an approach is that it results in a linear system of equations; however, the main drawback is that it introduces many more degrees of freedom into the solution space, which potentially adds to the non-uniqueness of the result. In our approach (based on Ji et al., 2002), we perform a joint, non-linear inversion of the geodetic and selected strong motion data to solve for the rise time, rupture initiation time and slip for each subfault. The benefit of this approach is the reduction in the number of free parameters.

In this report, we first provide an overview of the seismotectonic context of the Tohoku-Oki earthquake and some of its characteristics. We next describe the data set used in this study and the source model inverted from these data. We test the model by first comparing forward predicted tsunami waveforms and ground shaking with observations, which leads to the development of an enhanced source model to better match the observed higher frequency 3D ground motion response. We conclude with a discussion of the implications of our derived rupture model on the potential recurrence of such great events offshore northern Honshu.

* Corresponding author.
E-mail address: shjwei@caltech.edu (S. Wei).

0012-821X/$ - see front matter © 2012 Elsevier B.V. All rights reserved.
http://dx.doi.org/10.1016/j.epsl.2012.04.006

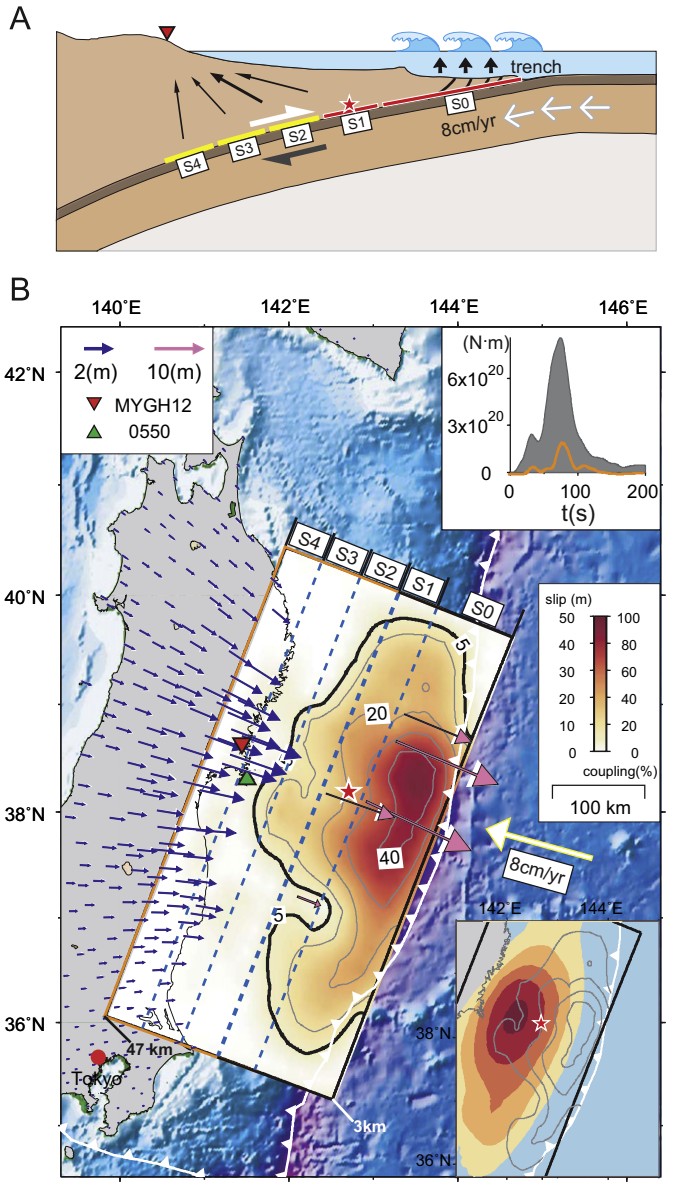

Fig. 1. Slip model of the Tohoku-Oki earthquake. (A) A cartoon displaying the subducting plate motion, tsunami generation and the partitioning of the fault plane. (B) Map view of the slip model, which is divided into 5 segments from shallow to deep (S0–S4), indicated by the dashed blue lines. These segments are defined for display purposes to show slip as a function of depth, and to clarify which parts of the fault contribute to which parts of the observed signals. The coseismic geodetic horizontal displacement vectors are displayed in white while the synthetics fits are presented in blue (inland) and pink (offshore). The differentials are small with misfit vectors given in the supplement. The heavy black and gray lines indicate the slip contours. The lower corner inset shows the interseismic coupling model assuming deep coupling only (Loveless and Meade, 2010) and the coseismic slip model (gray contours). The upper right inset displays the moment rate function for the whole slip model (gray) and the contribution from S2 to S4 (orange). The strong motion station MYGH12 and high-rate GPS station 0550 are indicated by red and green triangles, respectively. The red star indicates the epicenter. (For interpretation of the references to color in this figure legend, the reader is referred to the web version of this article.)

2. Source characteristics and seismotectonic context

There was little expectation that future interplate earthquakes along the eastern coast of Honshu would be different from the Mw < 8.5 earthquakes documented historically (Avouac, 2011). Moreover, the expectation was that future earthquakes would, like known past earthquakes, rupture areas confined to the patch of the plate interface that had remained locked in the interseismic period, as determined from the modeling of geodetic strain measured onshore (Hashimoto et al., 2009; Loveless and Meade, 2010; Suwa et al., 2006). These locked patches had been inferred to have limited extent in depth and laterally (Fig. 1B inset). In particular, the locked patch did not extend to depths shallower than about 10–15 km, a view consistent with the depth of the seismicity cut-off observed worldwide at subduction zone (Pacheco et al., 1993) and the notion that clay rich gouge along the shallow portion of the megathrust would favor aseismic slip (Hyndman et al., 1997). This is in keeping with the observations that the seismic rupture during recent well-documented mega-thrust events had not reached the trench (Konca et al., 2008, 2007; Sladen et al., 2010) with some having clearly triggered aseismic afterslip updip of the seismic rupture (Baba et al., 2006; Hsu et al., 2006). Also the 150×400 km^2 size of the locked patch suggested a low probability of Mw > 8.5 events given the scaling law between surface area and moment observed globally (Wesnousky, 2008). The Tohoku-Oki earthquake reached a moment magnitude of Mw = 9.0 (http://www.globalcmt.org/CMTsearch.html) which is about an 8 times larger moment than the largest previous earthquake known to have occurred there, the Sanriku earthquake of 1896 (Kanamori, 1972). The ratio of the moment to the surface area is much larger than observed globally. The main slip patch occurred close to the locked patch but was offset by about 50 km closer to the trench (Fig. 1B inset). Altogether these factors coalesced to generate an extraordinarily large tsunami.

Another interesting aspect of the Tohoku-Oki earthquake is that the shorter period (less than about 4–5 s) seismic energy appears to have originated primarily from the deeper part of the rupture, downdip of the hypocenter, despite the much larger moment released at shallow depth (Ishii, 2011; Koper et al., 2011; Meng et al., 2011; Wang and Mori, 2011; Yao et al., 2011; Zhang et al., 2011). Because of the dominance of the longer period energy in the geodetic and seismic data, it is difficult for our inversion to fully recover the shorter period aspects of the rupture process. We address this issue in the current work by adding short length scale (< 40 km) stochastic features to the inverted rupture model following the procedure outlined in Graves and Pitarka (2010). The resulting rupture model produces a significant improvement in the match to the observed pattern of strong motion amplitudes in the Tokyo Basin, particularly when we include the effects of 3D crustal structure in the wave propagation modeling.

3. Data resolution and joint inversion of seismic and geodetic data

Here we analyze the source of the earthquake in more detail to elucidate the causes for these various characteristics. We use static displacement offsets measured at 797 GPS stations on land (ARIA, processing of GSI data) and at 5 offshore locations near the epicenter (Sato et al., 2011). To constrain the slip history we use data from 14 accelerometer stations selected from the K-Net (http://www.k-net.bosai.go.jp/) and KiK-net (http://www.kik.bosai.go.jp/) which are well distributed along the coast (Fig. S1), see supplement for detail of this selection. We start with the Global Centroid Moment Tensor (GCMT) solution and adopt a rectangular fault plane, with an appropriate dip (10°) and strike (201°), as displayed in Fig. 1B. The fault plane is divided into a fine-grid of slipping patches parameterized by a slip-angle and offset, a rupture time (defined by an average rupture velocity from the hypocenter) and rise time. The rupture is assumed to initiate at the epicentral location (142.68°E, 38.19°N, 21 km) determined by Chu et al. (2011). To obtain the kinematic slip model, we adopt the inversion scheme developed by Ji et al. (2002). This method allows joint inversion of geodetic and seismic data by

setting different weights between the data sets. In this application we assumed equal weights for the total static and seismic data; this process is achieved by normalization of each misfit with the minimum error obtained by inverting each individual data set. All the parameters are inverted at the same time using a simulated annealing non-linear inversion scheme. During the inversion, the rupture velocity is constrained between 1 km/s and 2 km/s, as we apply in the checkerboard tests. Slip on the boundary grids for the bottom, the left side and the right side is forced to zero. Two extra constraints are applied, one that minimizes the slip differences between neighboring subfaults and a second that the total moment is fixed to the best long period double-couple moment as determined by the GCMT solution (5.31×10^{29} dyne cm). More inversion details could be found in the supplement.

Since all the inland GPS and seismic stations are located to one side of the epicenter, the resolution of these data decreases rapidly away from the coast, as has been noted previously (Loveless and Meade, 2011). Hence, we conducted a checkerboard test to investigate the importance of the 5 ocean bottom measurements on the data resolution. As displayed in Fig. 2, a checkerboard like slip distribution is used to generate synthetic data, accompanied by inverted slip distribution obtained with and without the 5 ocean bottom stations. The comparison demonstrates that the 5 ocean bottom data greatly improve the resolution for shallow slips especially for the slip patches near the sea floor stations. Since the inland static GPS data decays with distance faster than the seismic field it proves quite insensitive to the shallow rupture (Fig. 2C). In contrast, the seismic field contains the spatiotemporal information and alone has difficulty separating rise-time versus the amount of slip because the data is one-sided. Using the complete data set allows the resolution of both rupture velocity and rise-time as discussed in the supplement (Figs. S2 and S3). We also conducted tests to show the limited sensitivity of our results to the assumed slab geometry (Fig. S4 and S5).

Adopting the same inversion set up as used in the checkerboard tests, we inverted the real data sets resulting in the distribution of static slip shown in Fig. 1B and the timing results from modeling the waveforms shown in Fig. S6. The model fits to the static observations including the 5 ocean bottom measurements (Fig. 1B and Fig. S7) yield a variance reduction of 99.9% for horizontal components and 92.8% for vertical components. The inverted rupture model also provides a good fit to the longer period features of the strong motion records with an average cross-correlation coefficient of 0.82 (Fig. S8). The waveform comparison in Fig. S8 clearly indicates a deficiency in shorter period (<5 s) energy for our model, which is addressed in a later section. Our results indicate an extremely compact source with large slip (up to 50 m) at shallow depth. The moment release of the earthquake is dominated by this portion (Mw$\sim$9.0 for segments S0 and S1) as indicated in the upper right inset of Fig. 1B, corresponding to an average rupture velocity of $\sim$1.5 km/s (Fig. S6).

4. Forward predictions

Previous inversions discussed above lacked either the ocean bottom geodetic and and/or the refined epicenter location, where the largest slip occurred during the earthquake. In particular, shifting the epicenter by 30 km westward leads to distinctly different rupture properties (Chu et al., 2011). Thus the uniqueness of models becomes an essential issue. One of the best methods to examine the adequacy of the model involves the predictions, obtained from a given model, of observations not used in its construction. To this end, we analyze the predictions of sea floor uplift leading to flooding and the large data set of peak ground velocities and high rate GPS observations.

4.1. Tsunami excitation

As one test of our slip model we make a forward prediction for the 4 nearest Deep-ocean Assessment and Reporting of Tsunamis (DART) records using the vertical seafloor deformation (Fig. 3C). As in Fig. 1B, we separate the contributions of the slip model into shallow (S0–S1) and deeper (S2–S4) portions (Fig. 3A, B). Here we use the method developed by Wang and Liu (2007), and the seafloor uplift is treated as an instantaneous input. Because of the depth and the slip amplitude on S0 and S1, this portion produces the most seafloor deformation (Fig. 3A) and thus mainly fits the tsunami records (Fig. 3D). Since the tsunami data are plotted relative to the National Earthquake Information Center (NEIC) origin time, we applied a 90 s time delay for the synthetics to account for the difference between the beginning of the rupture and the time when maximum moment rate is achieved (Fig. 1B inset). In general, the synthetics predict the amplitude and the arrival times of the tsunami quite well although there is still some misfit to the shorter wavelength features particularly for stations 21401 and 21413. This could be due to details of the kinematic process of the earthquake near the trench and the dispersion of water wave propagation that are not taken into account in the current calculation.

4.2. Shaking estimates

Contrary to the tsunami, the ground shaking on Honshu appears to be controlled by the deeper portion of the rupture (Fig. 4). The strongest motions (period >2 s) at relatively hard rock sites occurred along the coast of the Miyagi Prefecture near the high-rate GPS station 0550 (Fig. 1B) and the nearby strong motion station MYGH12 with the dominant EW component shown in Fig. 4A. The peak motions for MYGH12 are 33 cm/s in the raw data, which was reduced to 21.5 cm/s when filtered to 2 s and longer as used in the inversion (Fig. 4B). Because of the difficulties in recovering the static offset from double integration of the strong motion recording we have also included the simulation of the nearby high-rate GPS as a prediction (Fig. 4C, D). Note that the large static offset occurred at about 70 s in the displacement record and is dominated by the strip S2. The upper portion (S0) contributes significantly to stations at further distances (Fig. S9 and S10). We generated forward predictions from Green's function separated into upgoing vs. downgoing energy release (Saikia and Helmberger, 1997) and found that the upgoing energy dominates the strong motions and the static field in the Tohoku region (Fig. 4A, C, D). Thus, the largest motions are coming from the direct SV wave generated by the strip S2 (Fig. 4B). Further evidence for this relatively simple explanation of these seismograms is given in a record section presented in Fig. S11.

We have generated synthetic predictions for all the high rate GPS stations with results summarized in Fig. S12 for the longer periods (>10 s) that are best constrained by the inversion. The synthetic EW component is the strongest and fits the observed waveforms with an average cross-correlation over 80%. The PGV simulated using hard rock (1D) Green's functions for various fault segments are given in Fig. 4H, I. Even though the upper portion (S0, S1) has the dominant moment release, it produces only weak ground motions, similar to those reported for the 1896 Sanriku Earthquake.

Generally, the longer the period the easier it is to model strong motions (Graves and Pitarka, 2010). The shorter period (2–10 s) pulses seen in the strong motion recording at MYGH12 (Fig. 4A) and other neighboring stations have timing that is consistent with the direct SV arrivals from S2 to S4. However, particle motion plots indicate these shorter period arrivals have a mixture of SV and SH motions, suggesting that we cannot explain such features without knowing the 3D velocity structure characterized by the shallow geological features. Because the waveforms are less coherent at periods less than about 8 s relative to the 1D Green's

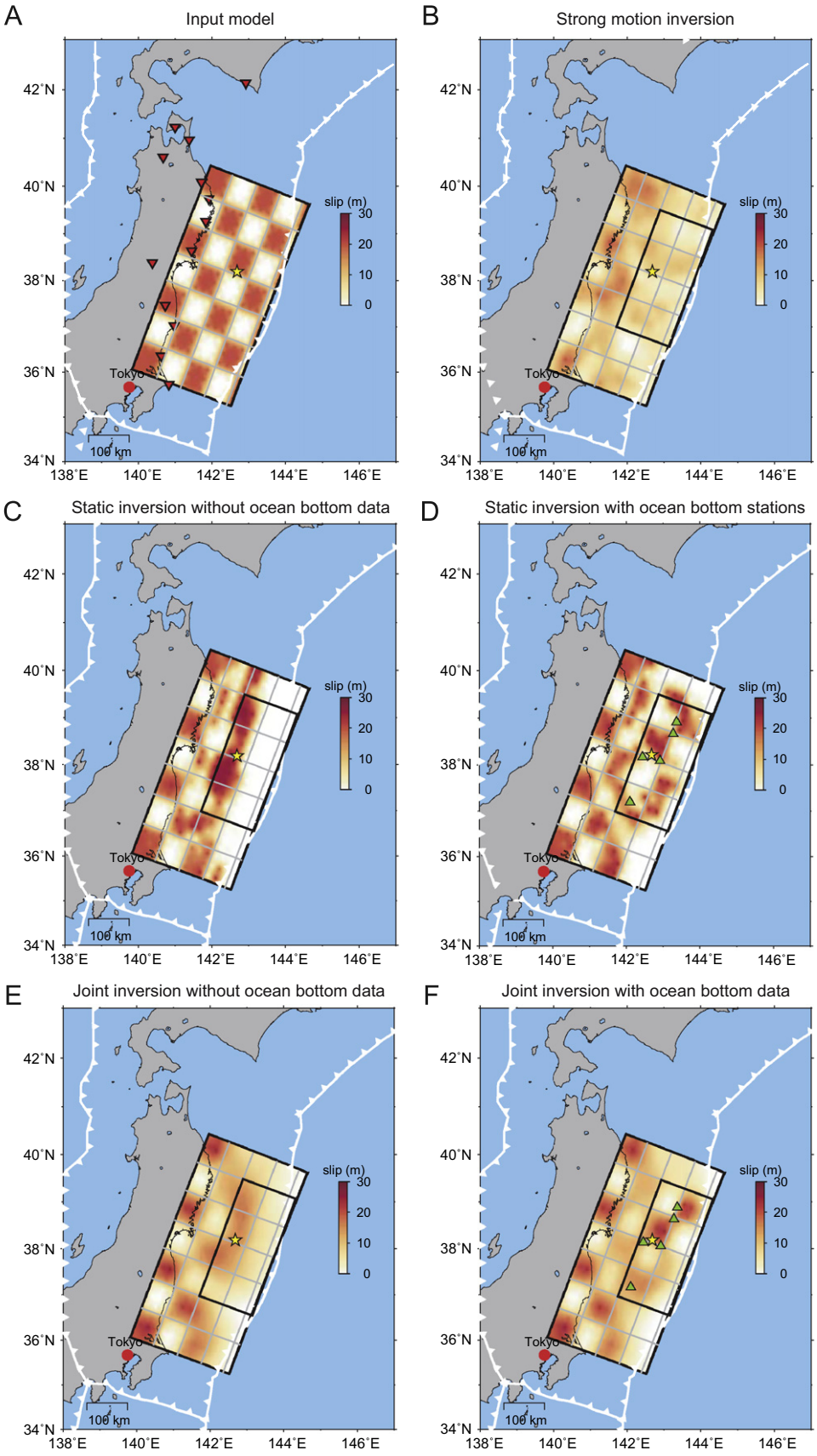

Fig. 2. Checkerboard tests for the model resolution. (A) The checkerboard slip model used to generate synthetic data where patches have no slip or 20 m of offset. Both seismic and static data are generated at stations recording the main event and used in the inversion. Red triangles indicate the strong motion stations. (B) The inversion results using only the strong motion data; results of static inversion in (C) and (D) and combined in (E) and (F). Green triangles indicate the ocean bottom geodetic station locations. (For interpretation of the references to color in this figure legend, the reader is referred to the web version of this article.)

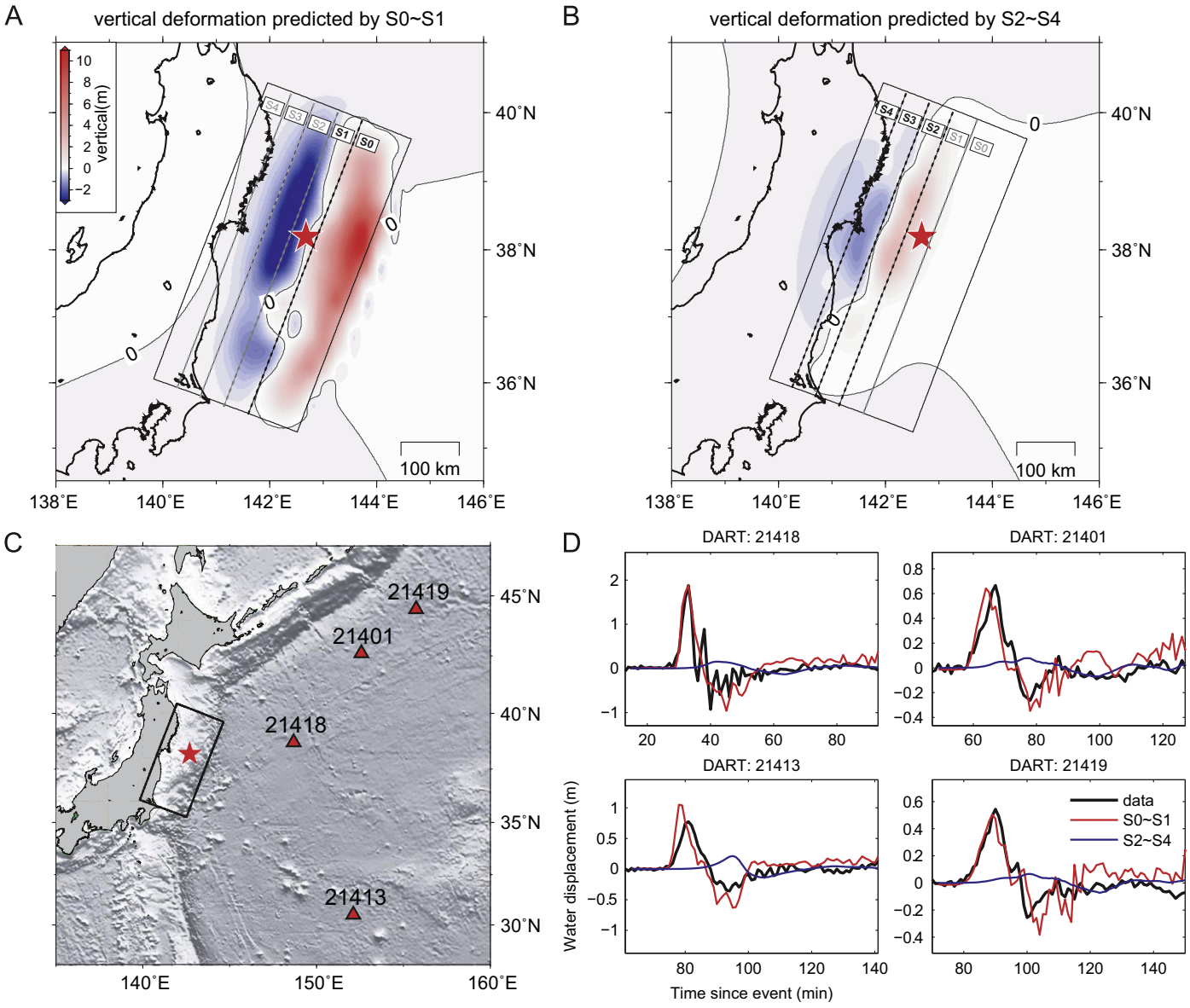

Fig. 3. Seafloor uplifts and prediction of open ocean tsunamis. Vertical seafloor deformation predicted by the slips in S0–S1 (A) and S2–S4 (B), the red star indicates the epicenter. (C) Map view of the location of four Deep-ocean Assessment and Reporting of Tsunamis (DART) stations, the epicenter and the fault plane are indicated by the star and rectangle, respectively. (D) DART record (black), prediction by the seafloor uplift from S0 to S1 (red) and S2–S4 (blue). The time axis is relative to the National Earthquake Information Center (NEIC) origin time and the synthetics are delayed by 90 s to account for the difference between the beginning of the rupture and the time when maximum moment rate is achieved (Fig. 1). (For interpretation of the references to color in this figure legend, the reader is referred to the web version of this article.)

functions, our inversion results are dominated by longer periods. This means that we cannot expect to see the observed shorter period complexity of peak-ground-velocity (PGV) evident in Fig. 4E and F where over 600 strong motion and ~400 high-rate GPS observations are summarized. The amplification pattern in both data sets shows a strong correlation with near surface geology (Fig. 4G), which is not reproduced by our simulation using only 1D Green's functions (Fig. 4H, I).

4.3. Predictions from 3D ground-motion simulations

Because the geology appears to be affecting the shorter period (<10 s) strong motions as displayed in Fig. 5A, we tested a 3D seismic velocity model for comparison with our simple 1D inversion results. The subsurface seismic velocity model is obtained from Japan's National Research Institute for Earth Science and Disaster Prevention (http://www.j-shis.bosai.go.jp/map/?lang=en) and represents the 3D structure of the upper (<16 km depth) crust, and includes many deep basin structures such as those in the Niigata and Tokyo regions (Fig. 4G). Fig. S13 displays the upper crustal complexity throughout the region considered in our modeling. We have capped the minimum shear wave velocity at 0.5 km/s (compared to 2.5 km/s used for the 1D model), and used a grid spacing of 0.4 km to obtain a reliable bandwidth of $T>4$ s for the 3D simulations (Graves, 1996). Our 3D simulation results compared to the observed PGV are given in Fig. 5. We performed two simulations using the 3D structural model. In the first simulation, we directly load the kinematic source model obtained from the 1D inversion into the 3D finite-difference grid. In the second simulation, we modify the shorter length-scale features of the inverted rupture model with the goal of enhancing the shorter-period energy radiated from the source prior to insertion into the 3D calculation.

The result from the first simulation is displayed in Fig. 5B. Even though these predictions are at relatively long period they still produce some amplification and extended motions for the deeper

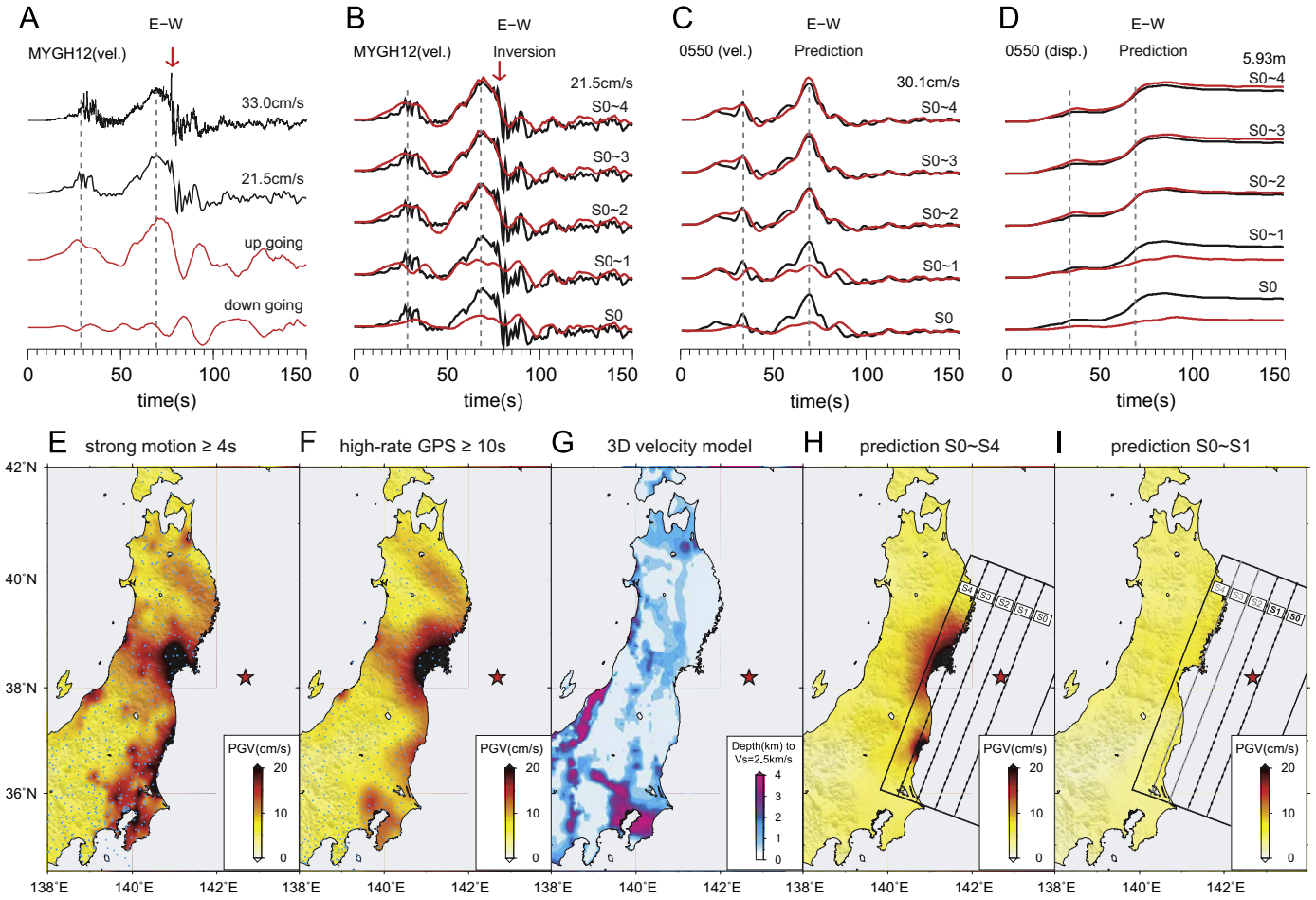

Fig. 4. Ground shaking produced by the earthquake and predictions of slip model. (A) From top to bottom are the E–W component of the velocity record (black) at the strong motion station MYGH12 and are plotted before and after filtering (≥ 2 s). The next two traces display the contributions from energy leaving the distributed sources in the upward direction vs. contribution from diving energy paths. The number at the end of each trace is the maximum amplitude. (B) The filtered data (black) is plotted along with the synthetics (red) generated cumulatively from S0 to S4. The data and synthetics are both low pass filtered (≥ 2 s). (C) Similar as (B) for the E–W velocity component at the high-rate GPS station 0550. The velocity data and synthetics are filtered (> 5 s). (D) Plots of the simulations in displacement at station 0550. (E) PGV (peak ground velocity) of strong motion records filtered to 4 s and longer. The triangles represent stations and the star indicates the epicenter location. (F) PGV of high-rate GPS (≥ 10 s) with triangles representing the stations. (G) Depth distribution of $Vs = 2.5$ km/s, the 3D velocity model is obtained from NIED. (H) PGV predicted by the whole slip model (S0–S4). (I) PGV predicted by upper portion of the slip model (S0 and S1). (For interpretation of the references to color in this figure legend, the reader is referred to the web version of this article.)

basins as displayed in Fig. 6. Most of the comparisons at hard rock sites show good agreement between 1D and 3D as given for the top set of traces, see Fig. S15 for more details. The 3D synthetics predict about the same fit to the entire network and yield compatible PGV to the 1D result (Fig. 5B vs. Fig. 4H). These results validate the adequacy of the 1D methodology used in the long period inversion.

One of the most noticeable differences in the observed waveforms at soft-rock vs. hard-rock sites is the length of coda and enhanced shorter periods seen at the soft-rock sites. As noted earlier, the rupture history assumed in our inversion approach is a simple, symmetric slip function, inset in Fig. 5C. While this assumption allows for more stable solutions and adds to their predictive ability at other sites, it tends to de-emphasize the shorter length-scale features of the slip distribution and is not compatible with high-frequency dynamic considerations where most dynamic models predict a Kostrov-like square root singularity at the faulting edge. These issues are addressed in a hybrid approach to continue the simple deterministic model into the higher frequency stochastic domain (Graves and Pitarka, 2010). Thus, in the second 3D simulation (Fig. 5C) we modify the source by (1) adding stochastic slip features at length scales less than 40 km, (2) constraining the average rise time on the shallow fault to be twice that for the deeper fault to replicate the transition from stable sliding to unstable sliding at a depth of 20 km (consistent with creeping depth for subduction zones (Hyndman et al., 1997)), and (3) replacing the smooth slip function with a Kostrov-like function (Fig. 5C inset) having an average rise time across the fault of 20 s (see Fig. S14 for details of this enhanced source simulation). The modified source increases the radiation of shorter period energy, particularly from the deeper portion of the fault and does better in predicting the spatial distribution of PGV, particularly for the basin regions as displayed in Fig. 5C. Additionally, the enhanced source produces much more later arriving coda at the basin sites, consistent with the observed motions. As expected, the tradeoff with this enhanced source is that the waveform fit to the main long period arrivals is slightly degraded at some sites compared to the original source (Fig. S15).

5. Rupture properties and interpretation

Due to the exceptional data quality we were able to constrain both the spatial (geodetic) and temporal variation of slippage as displayed in Fig. 7. Our model indicates that the earthquake had a relatively slow rupture velocity (~ 1.5 km/s on average over the first 80 s) as displayed in Fig. 7A. This is mainly constrained by the

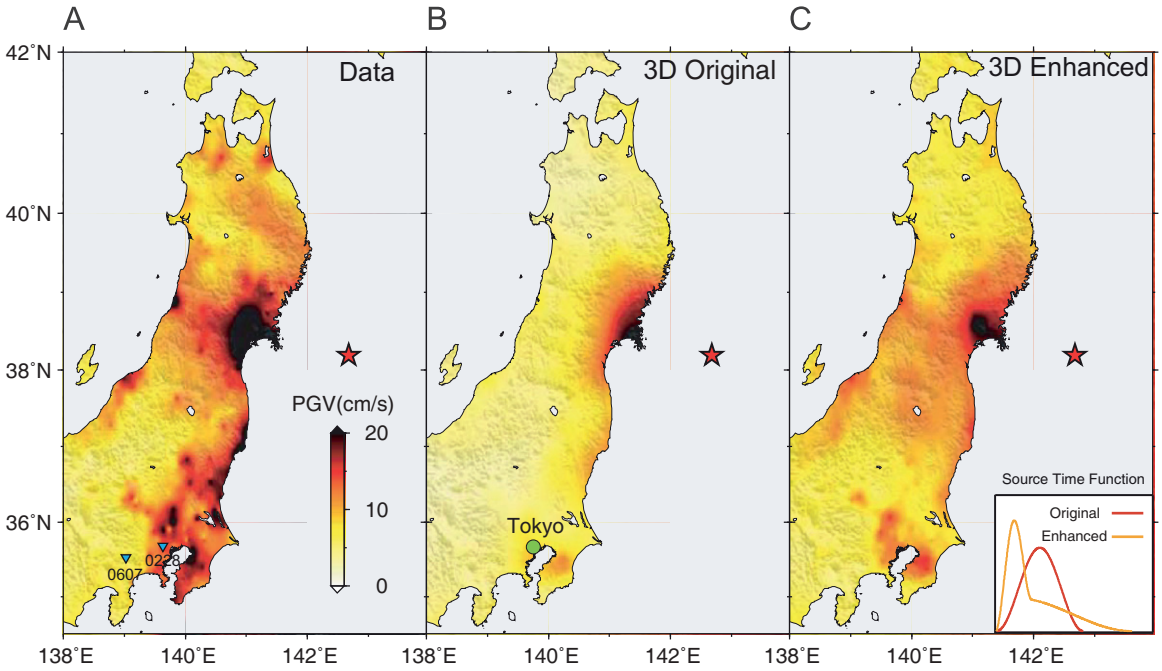

Fig. 5. Peak ground velocity (PGV) predictions by various slip models and velocity models. (A) PGV distribution derived from the combination of the strong motion and high-rate GPS data filtered to 4 s and longer. The two triangles indicate the high-rate GPS stations shown in Fig. 6. (B) PGV prediction by the original slip model and 3D velocity model. (C) PGV prediction from the revised slip model (rough) and 3D velocity model. The inset indicates the source time functions used for the predictions, see Fig. S14 for more details.

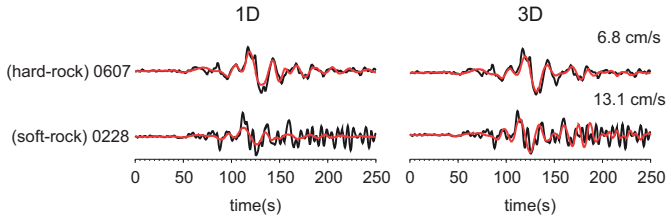

Fig. 6. Forward predictions for EW component of the two stations in (0228) and out (0607) of Tokyo Basin. The peak velocity of the data is indicated at the end of the trace. The 1D and 3D synthetics are calculated from the slip model obtained from the inversion. See Fig. S15 for more waveform comparisons at hard-rock vs. soft-rock sites.

long period strong motion data used in the inversion. On the other hand, other models, especially the back-projection results (Ishii, 2011; Koper et al., 2011; Meng et al., 2011; Wang and Mori, 2011; Yao et al., 2011; Zhang et al., 2011), indicate that the high frequency seismic radiation stayed near the hypocenter at the beginning stage of the rupture, before moving to the southwest and northeast. To address such issues requires more complexity in our present rupture formulation and incorporation of more high frequency data into the inversion; we will leave for the future efforts.

The rise times are displayed in Fig. S6 and the associated slip velocity is indicated in Fig. 7B. Generally there are strong trade-offs involving the slip velocity, slip distribution and rupture velocity (Konca et al., 2007). For these reasons various studies have reported different rise times depending on the frequencies used in their waveform inversion and the choice of event initiation, as well as the definition of rise time (i.e. Yokota et al., 2011; Yue and Lay, 2011). Checkerboard tests indicate that our estimates are resolvable, see Fig. S5. Our inversion produces rise times which correlate directly with slip (Fig. S6). The rise time (<25 s) is relatively short in comparison to source duration (120 s) suggesting a pulse-like rupture. The clear gradual increase of rise time as the rupture propagated upward suggests pulse broadening. However, the slip increases faster than rise time so that the slip velocity is larger at shallower depths (typically 2 m/s) than at deeper depths (0.5–1 m/s) (Fig. 7B). Note that the rise times are relatively short for the lower portion of the fault with patches of short rise times given is Fig. 7C. These patches appear to be related to the locations where higher frequency seismic waves are generated according to back-projection analyses (i.e. Meng et al., 2011). This small zone is special in several ways. First, it correlates with strong coupling, Fig. 7D; secondly it is void of repeating earthquakes (Uchida et al., 2002); and lastly it occurs in a high velocity tomographic image (Zhao et al., 2011). All these features suggest a strong zone resistant to faulting.

The observation of very large slip at shallow depth suggests that interseismic models published in the past may have underestimated the degree of locking of the shallow portion of the plate interface. On land geodetic data place rather weak constraints on the degree of locking at shallow depth and the inference of low coupling there was mostly due to the assumed boundary condition (zero coupling at the trench) and regularization of the inversions. Note, in the only instance where sea-bottom geodetic measurements are available, strong locking of shallow portion of the megathrust offshore Southern Peru has been inferred (Gagnon et al., 2005). Interseismic models which assume strong coupling at the trench actually fit the geodetic data just as well (Loveless and Meade, 2011), Fig. 7D. The area with strong locking now appears to correlate better with the rupture area of the Tohoku-Oki earthquake. This interseismic model could be considered as more realistic but it rises an issue: as seismic slip (and transient afterslip) needs to balance the deficit of slip accumulating in the interseismic period this model requires more frequent or larger seismic ruptures than models with lower coupling at shallow depth: the model in Fig. 7D would require Mw9.0 earthquake similar to Tohoku-Oki to recur in about every 400 yr (assuming that afterslip contributes 25% additional moment release) instead of $\sim$1000 yr for the model of Fig. 1B inset. Such a short return period is at odds with the observation that the penultimate large tsunamigenic earthquake occurred in 869AD (Minoura) and the >1000 yr return period of such events (Sawai et al., 2008). An alternative explanation would be

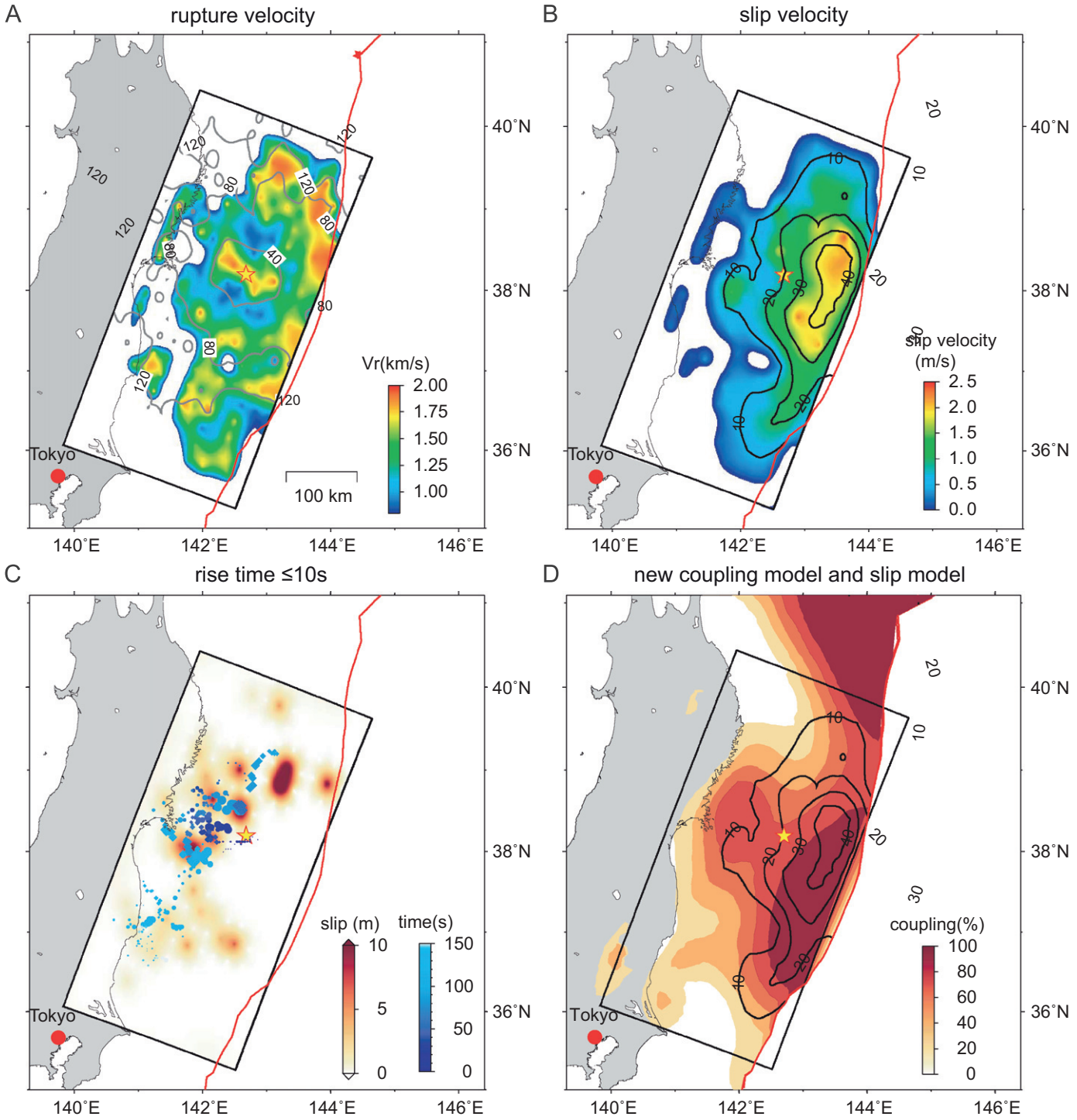

Fig. 7. Further details of variation in rupture velocities, rise-time distributions, slip velocity estimation and coupling. (A) Rupture velocity of the slip model with isochrones indicating the rupture time. (B) Slip velocity, defined as slip amplitude divided by rise time, is plotted along with coseismic slip contours. (C) Only the subfault slip with rise time ≤ 10 s are plotted, the blue circles (USArray) and squares (European Array) are the back-projection results colored by rupture time relative to the origin time with the size indicates the energy (Meng et al., 2011). (D) The coseismic slip contours (black lines) are overlapping on the top of a coupling model which allows strong locking near the trench (Loveless and Meade, 2011).

that the shallow portion of the plate interface would both creep aseismically and slip seismically on rare occasions.

Since our understanding of these huge tsunamigenic events is extremely limited, in particular due to their rarity and difficulty to constrain their characteristics in absence of this kind of data available for the Tohoku-Oki earthquake, it is worthwhile to speculate about the mechanisms involved in their occurrence based on the characteristics of this particularly well documented example. We note that during the Tohoku-Oki earthquake, the change-over to normal focal mechanism of aftershocks (Asano et al., 2011; Ide et al., 2011) indicate a nearly complete stress-drop on the upper fault portion (S0). This observation implies a very efficient dynamic weakening mechanism there. Given that this shallow portion of the plate interface is probably a place with abundant free water and low permeability, due to the large clay fraction in the sediments accumulated in the trench and dragged

along the megathrust, thermal pressurization (Sibson, 1973) could account for this strong weakening. Comparison with earthquakes sequence simulations by Noda and Lapusta (2010) is instructive in that regard. They consider two patches, A and B, side-by-side with distinct hydraulic diffusivity. The hydraulic diffusivity is lower within patch B allowing for thermal pressurization within that patch only. They find that most events nucleate in A and sometimes propagate into B where slip is enhanced due to thermal pressurization. As the rupture enters patch B the pulse grows broader, and the slip velocity increases. Because the final slip in patch B is much larger than in A, it ruptures less frequently. By analogy we propose that the shallow fault portion S0, where thermal pressurization might be favored, would rupture only occasionally in very large rupture (like patch B in the simulations of Noda and Lapusta (2010)) while deeper regions should rupture more frequently during more moderate events (like patch A of Noda and Lapusta, 2010). This would be consistent with the observation that large tsunamigenic earthquakes offshore Northern Honshu have very long return periods (>1000 yr), where more moderate earthquakes are much more frequent, with about 1 Mw >7.5 earthquake per decade over the last 120 yr. In short, such a theoretical framework provides one possible explanation of many aspects of the Tohoku-Oki earthquake.

6. Conclusions

We have been able to determine a source model of the Tohoku-Oki earthquake which explains the wide range of high quality data available for the earthquake, in particular ground motion from 10 s period to static, and the tsunami waveforms. A key aspect of our model is that the shallower and deeper portions of the rupture have fundamentally different characteristics. We propose that these differences are due to strong dynamic weakening process, possibly thermal pressurization, which produced large displacement rupture at shallow depth with little high frequency seismic radiation. The deeper rupture is characterized by relatively small fault displacement with relatively strong high frequency radiation, although we recognize that our current inversion approach has limited ability to resolve the details of these higher frequency features. However, we find that inclusion of 3-D propagation effects and enhancement of the high frequency features of the kinematic slip function provides an improved match to the observed ground motion response.

Acknowledgments

This research was supported by NSF Grant EAR-1142020 and USGS Award G10AP00048. Shengji Wei is supported in part under USGS Cooperative Agreement G09AC00150. Some of the large-scale 3D finite difference simulations were run at the University of Southern California's Center for High Performance Computing and Communications (http://www.usc.edu/hpcc) under an agreement with the SCEC Community Modeling Environment project. The high-rate GPS data, generously made available by C. Rocken of GPS Solutions, Inc. originated with efforts by GSI, NGDS, Hitz, GPSS and VERIPOS. Processed GPS time series are provided through the Caltech ARIA project. Strong motion waveforms were obtained from K-Net and KiK-Net of NIED. The Generic Mapping Tools (GMT) were used for creating the figures. We thank Morgan Page and Kenneth Hudnut for their comments.

Appendix A. Supporting information

Supplementary data associated with this article can be found in the online version at http://dx.doi.org/10.1016/j.epsl.2012.04.006.

References

Ammon, C.J., Lay, T., Kanamori, H., Cleveland, M., 2011. A rupture model of the 2011 off the Pacific coast of Tohoku Earthquake. Earth Planets Space 63, 693–696.
Asano, Y., Saito, T., Ito, Y., Shiomi, K., Hirose, H., Matsumoto, T., Aoi, S., Hori, S., Sekiguchi, S., 2011. Spatial distribution and focal mechanisms of aftershocks of the 2011 off the Pacific Coast of Tohoku Earthquake, Earth Planets Space. 10.5047/eps.2011.06.016.
Avouac, J.P., 2011. The lessons of Tohoku-Oki. Nature 475, 300–301, http://dx.doi.org/10.1038/nature10265.
Baba, T., Hirata, K., Hori, T., Sakaguchi, H., 2006. Offshore geodetic data conducive to the estimation of the afterslip distribution following the 2003 Tokachi-Oki earthquake. Earth Planet. Sci. Lett. 241, 281–292.
Chu, R.S., Wei, S.J., Helmberger, D., Kanamori, H., Zhan, Z.W., Zhu, L.P., 2011. Beginning of the great Mw=9.0 Tohoku-Oki earthquake. Earth Planet. Sci. Lett. 301, 277–283, http://dx.doi.org/10.1016/j.epsl.2011.06.03.
Fujii, Y., Satake, K., Sakai, S., Shinohara, M., Kanazawa, T., 2011. Tsunami source of the 2011 off the Pacific coast of Tohoku Earthquake. Earth Planets Space 63, 815–820.
Gagnon, K., Chadwell, C.D., Norabuena, E., 2005. Measuring the onset of locking in the Peru–Chile trench with GPS and acoustic measurements. Nature 434, 205–208.
Graves, R.W., 1996. Simulating seismic wave propagation in 3D elastic media using staggered grid finite differences. Bull. Seismol. Soc. Am. 86, 1091–1106.
Graves, R.W., Pitarka, A., 2010. Broadband ground-motion simulation using a hybrid approach. Bull. Seismol. Soc. Am. 100, 2095–2123.
Hashimoto, C., Noda, A., Sagiya, T., Matsu'ura, M., 2009. Interplate seismogenic zones along the Kuril–Japan trench inferred from GPS data inversion. Nature Geosci. 2, 141–144.
Hayashi, Y., Tsushima, H., Hirata, K., Kimura, K., Maeda, K., 2011. Tsunami source area of the 2011 off the Pacific coast of Tohoku Earthquake determined from tsunami arrival times at offshore observation stations. Earth Planets Space 63, 809–813.
Hayes, G.P., 2011. Rapid source characterization of the 2011 M(w) 9.0 off the Pacific coast of Tohoku Earthquake. Earth Planets Space 63, 529–534.
Hsu, Y.J., Simons, M., Avouac, J.P., Galetzka, J., Sieh, K., Chlieh, M., Natawidjaja, D., Prawirodirdjo, L., Bock, Y., 2006. Frictional afterslip following the 2005 Nias–Simeulue earthquake, Sumatra. Science 312, 1921–1926.
Hyndman, R.D., Yamano, M., Oleskevich, D.A., 1997. The seismogenic zone of subduction thrust faults. The Island Arc 6, 244–260.
Ide, S., Baltay, A., Beroza, G.C., 2011. Shallow dynamic overshoot and energetic deep rupture in the 2011 M-w 9.0 Tohoku-Oki earthquake. Science 332, 1426–1429.
Ishii, M., 2011. High-frequency rupture properties of the M(w) 9.0 off the Pacific coast of Tohoku Earthquake. Earth Planets Space 63, 609–614.
Ji, C., Wald, D.J., Helmberger, D.V., 2002. Source description of the 1999 Hector Mine, California, earthquake, part I: wavelet domain inversion theory and resolution analysis. Bull. Seismol. Soc. Am. 92, 1192–1207.
Kanamori, H., 1972. Mechanism of tsunami earthquakes. Phys. Earth Planet. Int. 6, 346–359.
Koketsu, K., Yokota, Y., Nishimura, N., Yagi, Y., Miyazaki, S., Satake, K., Fujii, Y., Miyake, H., Sakai, S., Yamanaka, Y., Okada, T., 2011. A unified source model for the 2011 Tohoku earthquake. Earth Planet. Sci. Lett. 310, 480–487.
Konca, A.O., Avouac, J.P., Sladen, A., Meltzner, A.J., Sieh, K., Fang, P., Li, Z.H., Galetzka, J., Genrich, J., Chlieh, M., Natawidjaja, D.H., Bock, Y., Fielding, E.J., Ji, C., Helmberger, D.V., 2008. Partial rupture of a locked patch of the Sumatra megathrust during the 2007 earthquake sequence. Nature 456, 631–635.
Konca, A.O., Hjorleifsdottir, V., Song, T.R.A., Avouac, J.P., Helmberger, D.V., Ji, C., Sieh, K., Briggs, R., Meltzner, A., 2007. Rupture kinematics of the 2005 M-w 8.6 Nias-Simeulue earthquake from the joint inversion of seismic and geodetic data. Bull. Seismol. Soc. Am. 97, S307–S322.
Koper, K.D., Hutko, A.R., Lay, T., Ammon, C.J., Kanamori, H., 2011. Frequency-dependent rupture process of the 2011 M(w) 9.0 Tohoku Earthquake: comparison of short-period P wave backprojection images and broadband seismic rupture models. Earth Planets Space 63, 599–602, http://dx.doi.org/10.5047/eps.2011.05.026.
Kurahashi, S., Irikura, K., 2011. Source model for generating strong ground motions during the 2011 off the Pacific coast of Tohoku Earthquake. Earth Planets Space 63, 571–576.
Lay, T., Bilek, S., 2006. Anomalous earthquake ruptures at shallow depths on subduction zone megathrusts. In: Dixon, T.H., Moore, C. (Eds.), The Seismogenic Zone of Subduction Thrust Faults. Columbia University Press, pp. 476–511.
Lay, T., Yamazaki, Y., Ammon, C.J., Cheung, K.F., Kanamori, H., 2011. The 2011 M(w) 9.0 off the Pacific coast of Tohoku Earthquake: comparison of deep-water tsunami signals with finite-fault rupture model predictions. Earth Planets Space 63, 797–801.
Lee, S.J., Huang, B.S., Ando, M., Chiu, H.C., Wang, J.H., 2011. Evidence of large scale repeating slip during the 2011 Tohoku-Oki earthquake. Geophys. Res. Lett., 38.
Loveless, J.P., Meade, B.J., 2010. Geodetic imaging of plate motions, slip rates, and partitioning of deformation in Japan. J. Geophys. Res., 115, http://dx.doi.org/10.1029/2008JB006248.
Loveless, J.P., Meade, B.J., 2011. Spatial correlation of interseismic coupling and coseismic rupture extent of the 2011 Mw=9.0 Tohoku-oki earthquake, Geophys. Res. Lett.. 10.1029/2011GL048561.

Maeda, T., Furumura, T., Sakai, S., Shinohara, M., 2011. Significant tsunami observed at ocean-bottom pressure gauges during the 2011 off the Pacific coast of Tohoku Earthquake. Earth Planets Space 63, 803–808.

Meng, L.S., Inbal, A., Ampuero, J.P., 2011. A window into the complexity of the dynamic rupture of the 2011 Mw 9 Tohoku-Oki earthquake. Geophys. Res. Lett., 38.

Noda, H., Lapusta, N., 2010. Three-dimensional earthquake sequence simulations with evolving temperature and pore pressure due to shear heating: effect of heterogeneous hydraulic diffusivity. J. Geophys. Res., 115.

Ozawa, S., Nishimura, T., Suito, H., Kobayashi, T., Tobita, M., Imakiire, T., 2011. Coseismic and postseismic slip of the 2011 magnitude-9 Tohoku-Oki earthquake, Nature. 10.1038/Nature10227.

Pacheco, J.F., Sykes, L.R., Scholz, C.H., 1993. Nature of seismic coupling along simple plate boundaries of the subduction type. J. Geophys. Res. 98, 14133–14159.

Saikia, C.K., Helmberger, D.V., 1997. Approximation of rupture directivity in regional phases using upgoing and downgoing wave fields. Bull. Seismol. Soc. Am. 87, 987–998.

Saito, T., Ito, Y., Inazu, D., Hino, R., 2011. Tsunami source of the 2011 Tohoku-Oki earthquake, Japan: inversion analysis based on dispersive tsunami simulations. Geophys. Res. Lett., 38.

Sato, M., Ishikawa, T., Ujihara, N., Yoshida, S., Fujita, M., Mochizuki, M., Asada, A., 2011. Displacement above the hypocenter of the 2011 Tohoku-Oki earthquake. Science 332. 1395–1395.

Sawai, Y., Fujii, Y., Fujiwara, O., Kamataki, T., Komatsubara, J., Okamura, Y., Satake, K., Shishikura, M., 2008. Marine incursions of the past 1500 years and evidence of tsunamis at Suijin-numa, a coastal lake facing the Japan Trench. Holocene 18, 517–528.

Shao, G.F., Li, X.Y., Ji, C., Maeda, T., 2011. Focal mechanism and slip history of the 2011 M(w) 9.1 off the Pacific coast of Tohoku Earthquake, constrained with teleseismic body and surface waves. Earth Planets Space 63, 559–564.

Sibson, R.H., 1973. Interactions between temperature and pore-fluid pressure during earthquake faulting and a mechanism for partial or total stress relief. Nat. Phys. Sci. 243, 66–68.

Simons, M., Minson, S.E., Sladen, A., Ortega, F., Jiang, J.L., Owen, S.E., Meng, L.S., Ampuero, J.P., Wei, S.J., Chu, R.S., Helmberger, D.V., Kanamori, H., Hetland, E., Moore, A.W., Webb, F.H., 2011. The 2011 magnitude 9.0 Tohoku-Oki earthquake: mosaicking the megathrust from seconds to centuries. Science 332, 1421–1425.

Sladen, A., Tavera, H., Simons, M., Avouac, J.P., Konca, A.O., Perfettini, H., Audin, L., Fielding, E.J., Ortega, F., Cavagnoud, R., 2010. Source model of the 2007 M(w) 8.0 Pisco, Peru earthquake: implications for seismogenic behavior of subduction megathrusts. J. Geophys. Res., 115, http://dx.doi.org/10.1029/2009JB006429.

Suwa, Y., Miura, S., Hasegawa, A., Sato, T., Tachibana, K., 2006. Interplate coupling beneath NE Japan inferred from three-dimensional displacement field. J. Geophys. Res., 111, http://dx.doi.org/10.1029/2004JB003203.

Suzuki, W., Aoi, S., Sekiguchi, H., Kunugi, T., 2011. Rupture process of the 2011 Tohoku-Oki mega-thrust earthquake (M9.0) inverted from strong-motion data. Geophys. Res. Lett., 38.

Tsushima, H., Hirata, K., Hayashi, Y., Tanioka, Y., Kimura, K., Sakai, S., Shinohara, M., Kanazawa, T., Hino, R., Maeda, K., 2011. Near-field tsunami forecasting using offshore tsunami data from the 2011 off the Pacific coast of Tohoku Earthquake. Earth Planets Space 63, 821–826.

Uchida, N., Igarashi, T., Matsuzawa, T., Hasegawa, A., 2002. Spatio-temporal distribution of interplate quasi-static slip in the northeastern Japan subduction zone, estimated from repeating earthquake analyses. EOS Trans. AGU 83, 47.

Wang, D., Mori, J., 2011. Rupture process of the 2011 off the Pacific coast of Tohoku Earthquake (M(w) 9.0) as imaged with back-projection of teleseismic P-waves. Earth Planets Space 63, 603–607, http://dx.doi.org/10.5047/eps.2011.05.029.

Wang, X.M., Liu, P.L.F., 2007. Numerical simulations of the 2004 Indian Ocean tsunamis—coastal effects. J. Earthquake Tsunami 1, 273–297.

Wesnousky, S.G., 2008. Displacement and geometrical characteristics of earthquake surface ruptures: issues and implications for seismic-hazard analysis and the process of earthquake rupture. Bull. Seismol. Soc. Am. 98, 1609–1632.

Yagi, Y., Fukahata, Y., 2011. Rupture process of the 2011 Tohoku-oki earthquake and absolute elastic strain release. Geophys. Res. Lett., 38.

Yamazaki, Y., Lay, T., Cheung, K.F., Yue, H., Kanamori, H., 2011. Modeling near-field tsunami observations to improve finite-fault slip models for the 11 March 2011 Tohoku earthquake. Geophys. Res. Lett., 38.

Yao, H.J., Gerstoft, P., Shearer, P.M., Mecklenbrauker, C., 2011. Compressive sensing of the Tohoku-Oki Mw 9.0 earthquake: frequency-dependent rupture modes. Geophys. Res. Lett., 38.

Yokota, Y., Koketsu, K., Fujii, Y., Satake, K., Sakai, S., Shinohara, M., Kanazawa, T., 2011. Joint inversion of strong motion, teleseismic, geodetic, and tsunami datasets for the rupture process of the 2011 Tohoku earthquake. Geophys. Res. Lett., 38.

Yoshida, K., Miyakoshi, K., Irikura, K., 2011. Source process of the 2011 off the Pacific coast of Tohoku Earthquake inferred from waveform inversion with long-period strong-motion records. Earth Planets Space 63, 577–582.

Yue, H., Lay, T., 2011. Inversion of high-rate (1 sps) GPS data for rupture process of the 11 March 2011 Tohoku earthquake (M(w) 9.1). Geophys. Res. Lett., 38.

Zhang, H., Ge, Z.X., Ding, L.Y., 2011. Three sub-events composing the 2011 off the Pacific coast of Tohoku Earthquake (M(w) 9.0) inferred from rupture imaging by back-projecting teleseismic P waves. Earth Planets Space 63, 595–598.

Zhao, D.P., Huang, Z., Umino, N., Hasegawa, A., Kanamori, H., 2011. Structural heterogeneity in the megathrust zone and mechanism of the 2011 Tohoku-oki earthquake (Mw 9.0), Geophys. Res. Lett.. 10.1029/2011GL048408.